Optics Letters

Cryogenic lithium-niobate-on-insulator optical filter

Yujie Cheng,[1,2] Lantian Feng,[1,2,*] Jianghao He,[3] Xinyu Song,[1,2] Xu Han,[4] Yuyang Ding,[5] Cheng Wang,[6] Guangcan Guo,[1,2] Ming Zhang,[3,7] Daoxin Dai,[3,8] and Xifeng Ren[1,2]

[1]CAS Key Laboratory of Quantum Information, University of Science and Technology of China, Hefei 230026, China
[2]CAS Synergetic Innovation Center of Quantum Information & Quantum Physics, University of Science and Technology of China, Hefei 230026, China
[3]Key Laboratory for Modern Optical Instrumentation, Centre for Optical and Electromagnetic Research, Zhejiang Provincial Key Laboratory for Sensing Technologies, Zhejiang University, Zijingang Campus, Hangzhou 310058, China
[4]School of Instrument Science and Opto-electronics Engineering, Hefei University of Technology, Hefei 230009, China
[5]Hefei Guizhen Chip Technologies Co., Ltd., Hefei 230000, China
[6]Department of Electrical Engineering and State Key Laboratory of Terahertz and Millimeter Waves, City University of Hong Kong, Kowloon, Hong Kong SAR, China
[7]mingzhang@zju.edu.cn
[8]dxdai@zju.edu.cn
*fenglt@ustc.edu.cn

Received 12 January 2024; revised 19 March 2024; accepted 24 March 2024; posted 25 March 2024; published 5 April 2024

Photonic integrated circuits have garnered significant attention and experienced rapid development in recent years. To provide fundamental building blocks for scalable optical classical and quantum information processing, one important direction is to develop cryogenic compatible photonic integrated devices. Here, we prepare one optical filter on a lithium-niobate-on-insulator (LNOI) platform based on a multimode waveguide grating and verify its availability at temperature from 295 to 7 K. We find that the integrated optical filter still shows good quality under cryogenic conditions, and the shift of the working wavelength at different temperatures is well explained by the index variation of the material. These results advance LNOI integrated optical devices in applications under cryogenic conditions.

https://doi.org/10.1364/OL.518418

Photonic integrated circuits (PICs) integrate multiple optical modules on one single chip and have developed into a compelling platform to providing fundamental elements for a wide range of classical and quantum information applications [1–3]. While most investigations on PICs have focused on the performance at ambient temperatures, cryogenic photonic components have become increasingly important in recent years. First, superconducting nanowire single-photon detectors, which have been widely used in applications such as quantum information processing [4–7] and deep space communication [8], generally require operation at cryogenic temperatures. Second, whether multiple cryogenic quantum processors connect over large distances [9,10] or realize digital data transfer between cryogenic processors and the room-temperature environment [11], photonic technologies are essential for future generations of scalable communication and computing networks. In addition, the manipulation of deterministic single-photon sources [12] or trapped ions [13] all depend on the development of cryogenic photonic technologies.

Currently, cryogenic nonlinear processes [14–16]and active modulators [17–20] have received much attention and a lot of research; however, the temperature-dependent responses of passive devices have made little progress. While some simple structures such as beam splitters [21] have been shown to still work at low temperatures, the cryogenic compatibility of devices with more complex functions such as filters and isolators requires a cautious attitude. The cryogenic environment will alter the refractive index, absorption, emission, and scattering properties of the material, thus affecting the reliability and efficiency of photonic devices and increasing the difficulty in constructing large-scale PICs. For example, the response of the resonator-based optical filter in silicon [22] is extremely sensitive to the temperature. Therefore, exploring the properties of cryogenic compatible optical devices is imperative, and more attention should be paid to optical integrated module's property and performance under cryogenic conditions.

In this work, we prepare one optical filter on lithium-niobate-on-insulator (LNOI) platform and study its performance with the influence of temperature. As one of the most promising platforms for integrated photonics, the LNOI waveguide offers excellent material properties, such as large electro-optic, acousto-optic, and nonlinear coefficients, wide transmission window, and high laser damage threshold, which make it suitable for preparing various optical devices [23–26]. The optical filter acts as a basic optical module to select specific wavelengths and transmit or block them and is widely used in classical and quantum information applications. Although the refractive index variation of the bulk lithium niobate at different temperatures has been explored [27], the research on the performance of LN integrated nano-devices at cryogenic temperatures is still lacking. The optical filter response at different temperatures will give us a better understanding of the properties of the LNOI waveguide, and the cryogenic compatible optical filter will further increase the application scenarios of LNOI devices with frequency control capability.

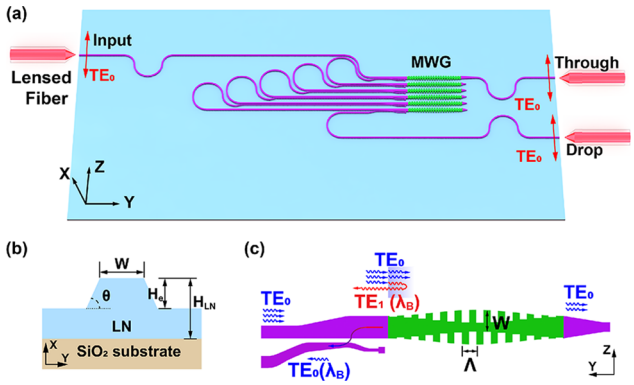

Fig. 1. Schematic configurations. (a) Image of the lithium-niobate-on-insulator optical filter chip with input and output ports on its left and right sides. Six MWGs were cascaded to achieve enough isolation ratio. (b) Waveguide's cross section with key parameters marked. (c) Image of the detailed MWG and mode (de)multiplexer structure. The mode (de)multiplexers enable efficient and broadband mode conversion between the TE_0 and TE_1 mode. MWG, multimode waveguide grating.

The optical filter is designed and fabricated based on the multimode waveguide grating as demonstrated in Ref. [28], and we further prove experimentally that it can work at cryogenic temperatures. We show that the bandwidths, shape factors, and isolation of the filter remain mostly unchanged ranging from room temperature to cryogenic temperature. Its center wavelength exhibits a temperature-dependent shift, decreasing by approximately 4 nm at cryogenic temperature (7 K) compared to the results at room temperature (295 K). Through introducing the temperature-dependent effective index of the grating structure in the filter for further analysis, the center wavelength shift with temperature is explained. Our results will guide the design of LNOI devices operable at cryogenic temperatures and increasing the potential of LNOI photonics under cryogenic conditions.

Here, we use the LN nanophotonics waveguide and multimode waveguide grating (MWG) to develop the cryogenic compatible optical filter. It was designed and fabricated based on the x-cut LNOI wafer from the NANOLN company. Figure 1(a) shows the schematic configuration of the device, and it has a dimension of 0.2×1.2 mm^2. In the experiment, on-chip end couplers were used to couple in/out the laser and lensed fibers were employed for coupling. The LN thickness is 400 nm and the etching depth is 200 nm with the sidewall angle $\theta = 72°$ [Fig. 1(b)]. In the single-mode region, the core width W is 1 μm. While in the MWG region, the core width is 2 μm. All devices were designed to work with the TE mode, and the guided wave propagated along the y axis direction. When the laser with the fundamental mode TE_0 enters the waveguide, the MWG in the core regime of the device will reflect the laser with a specific wavelength λ_B and convert it into the first higher-order mode TE_1 [Fig. 1(c)]. The wavelength λ_B satisfies the following formula [29]:

$$\lambda_B = (n_{eff0} + n_{eff1})\,\Lambda, \tag{1}$$

where n_{eff0} and n_{eff1} are the effective refractive indices of the TE_0 and TE_1 modes in the MWG, respectively, and Λ is the grating period. The follow-up mode demultiplexer enables efficient and broadband mode conversion and converts the reflected TE_1 mode into the TE_0 mode [30]. For those wavelengths away from λ_B, Eq. (1) is not satisfied, and the input laser will directly pass through the multimode waveguide with ultra-low loss. Thus, the MWG acts as a passband filter with the center wavelength λ_B. In order to ensure the working wavelength around 1550 nm, we set the grating period of the MWG $\Lambda = 436.00$ nm with a duty cycle of 50%, and the MWG has a dimension of 0.05×0.5 mm^2. Besides, six MWGs were cascaded to achieve enough isolation ratio. More details about chip design and fabrication can be found in Ref. [28]. Below we give the theoretical analysis of the optical filter's response to the temperature variation.

Temperature may change the dimension of the device and the refractive index of the material. However, due to the extremely tiny thermal expansion coefficients of LN, which is on the order of 10^{-6}/K [31], the grating period variation due to the thermal expansion of the material is estimated to be less than 0.2%, and the variation of the cross section of the device at different temperatures can be considered insignificant. The response variation of the optical filter can be considered to be mainly caused by the mode index discrepancy at different temperatures.

To accurately obtain the refractive indices of the TE_0 mode and the TE_1 mode in the MWG, we first ascertained how the material's refractive index changes with temperature. For the LN device designed with the x-cut and y-propagation configuration, the refractive index of the TE_0 and TE_1 modes are solely tied to the extraordinary refractive index (i.e., n_e) of the material. The variation of n_e with temperature is described by the Sellmeier equation [32]:

$$n_e^2 = a_1 + b_1 f + \frac{a_2 + b_2 f}{\lambda^2 - (a_3 + b_3 f)^2} + \frac{a_4 + b_4 f}{\lambda^2 - a_5^2} - a_6 \lambda^2, \tag{2}$$

where the wavelength λ has the unit of μm and f is given by

$$\begin{aligned} f &= (T - T_0)\,(T + T_0 + 2 \times 273.16) \\ &= (T - 24.5°\mathrm{C})\,(T + 570.82). \end{aligned} \tag{3}$$

Here, the temperature T is expressed in kelvins. The Sellmeier coefficients are $a_1 = 5.35583$, $a_2 = 0.100473$, $a_3 = 0.20692$, $a_4 = 100$, $a_5 = 11.34927$, $a_6 = 1.5334 \times 10^{-2}$, $b_1 = 4.629 \times 10^{-7}$, $b_2 = 3.862 \times 10^{-8}$, $b_3 = -0.89 \times 10^{-8}$, and $b_4 = 2.657 \times 10^{-5}$. Though these coefficients were verified for wavelengths ranging from 0.4 to 5 μm and temperatures between room temperature and 250°C in Ref. [32], the refractive indices in the range from 7 to 295 K still can be approximated based on this formula. We calculated the temperature-dependent variation of extraordinary index n_e in the range of 7–295 K, as shown in Fig. 2(a).

Based on the material's refractive index n_e, we further calculated the effective mode refractive indices of the TE_0 and TE_1 modes in the MWG with different temperatures by using the 3D FDTD method (Lumerical). The results are depicted in Fig. 2(b). We can see that the cryogenic cooling decreases the material and transverse mode indices and thus changes the performance of the optical filter. However, even at temperature down to 7 K, the TE_0 and TE_1 modes in the MWG are still stably supported and transmitted. The energy distributions of the TE_0 and TE_1 modes in the MWG at 7 K are shown in Figs. 2(c) and 2(d).

As shown in Fig. 3, in the experiment, we used a C-band amplified spontaneous emission (ASE) broadband laser to characterize the optical filter, which has an approximately flat spectrum across the wavelength range of 1529 to 1565 nm. By using the lensed fiber (Corning SMF-28E+LL) with a mode

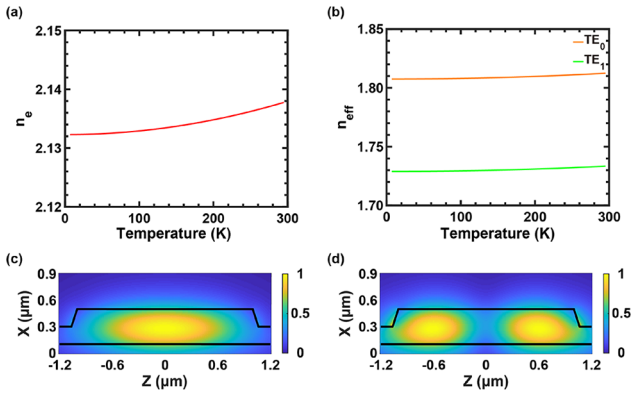

Fig. 2. Simulations and calculations. (a) Variation of the extraordinary light refractive index n_e of the material with temperature. (b) Variation of the effective mode refractive indices for the TE_0 and TE_1 modes with temperature. (c) and (d) Energy distributions of the modes TE_0 and TE_1 at 7 K.

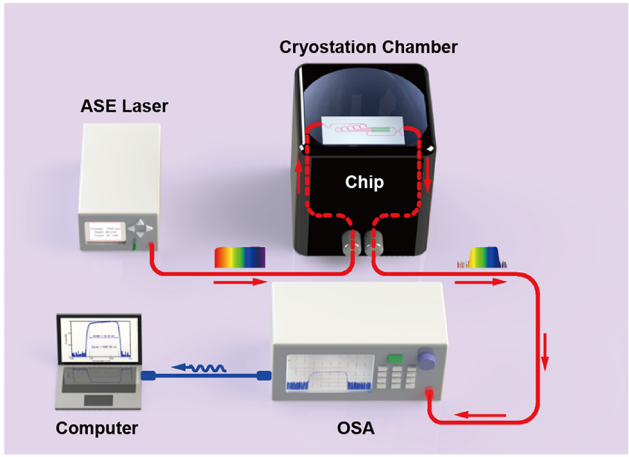

Fig. 3. Experimental setup with the on-chip lithium-niobate-on-insulator optical filter placed in the cryostation chamber. The data was obtained by the OSA and further analyzed by one personal computer. ASE laser, amplified spontaneous emission laser; OSA, optical spectrum analyzer.

field diameter of 2.5 μm, chip–fiber coupling with single-end 8 dB coupling loss was achieved. In the test, the chip and lensed fibers were placed in the cryostation sample chamber (Montana Instruments), which can control the temperature to any values between 7 K and room temperature with a control precision of 20 mK. In the chamber, interior displacement stages were used to adjust the position of lensed fibers to maintain the coupling efficiency during the test. At last, the output signal from the filter was directed to one optical spectrum analyzer (OSA, Yokogawa) for recording and analysis.

Through cooling the device to 7 K, we first characterized the optical filter under cryogenic conditions. We recorded the outputs at the drop and through port, respectively, and the results are given in Figs. 4(a) and 4(b). For comparison, the results recorded at room temperature are also given. To reduce the impact of random error, five sets of data were collected at the same port and same temperature, and the averaged results are given. Besides, the results were normalized based on the ASE's

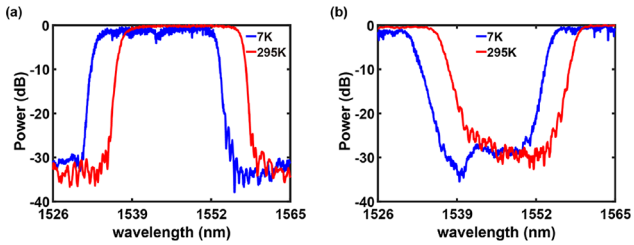

Fig. 4. Normalized spectra measured by the OSA. (a) Spectra at 7 and 295 K obtained at the drop port. (b) Spectra at 7 and 295 K obtained at the through port.

spectrum. We can see that even under cryogenic conditions, the optical filter still has basically the same performance as that at room temperature, such as approximately 30 dB isolation ratio and similar bandwidth. Specifically, at 7 K, the spectrum at the drop port has the center wavelength of 1543.02 ± 0.12 nm and a bandwidth of 19.24 ± 0.17 nm, and the spectrum at the through port has the center wavelength of 1543.18 ± 0.07 nm and a bandwidth of 22.76 ± 0.13 nm. At 295 K, the spectrum at the drop port has the center wavelength of 1547.22 ± 0.01 nm and a bandwidth of 19.48 ± 0.02 nm, and the spectrum at the through port has the center wavelength of 1547.40 ± 0.00 nm and a bandwidth of 22.56 ± 0.00 nm. We also calculated the filter's shape factor, which is defined as the ratio of −1 dB to −10 dB bandwidths, to assess the optical filter's box-like quality [33]. The shape factor is unity for the ideal rectangular filter. At 7 K, the shape factor of the spectrum at the drop port is 0.81 ± 0.08 and that at the through port is 0.81 ± 0.01. At 295 K, the shape factor of the spectrum at the drop port is 0.82 ± 0.00 and that at the through port is 0.83 ± 0.00. At 7 K, the isolation ratio for the spectra at the drop port is 29.96 ± 0.20 dB and 25.20 ± 0.07 dB for the results at the through port. At 295 K, the isolation ratio is 30.55 ± 0.06 dB at the drop port and 24.78 ± 0.01 dB at the through port. Here, the errors are obtained by the multiple measurements. We can conclude from these results that except the small shift of the filter's center wavelength, the optical filter shows basically the same performance under cryogenic conditions.

To better describe the relationship between the response of the optical filter and the temperature, we further recorded and analyzed multiple parameters of the optical filter at different temperatures. Figure 5 shows how the bandwidth, shape factor, and center wavelength of the spectra change with the temperature. For the bandwidth and shape factor shown in Figs. 5(a) and 5(b), we can see that both values fluctuate along straight lines, and the error bars are mainly from the vibration of the test platform. For the center wavelength shown in Fig. 5(c), we observed a significant increase as the temperature rises, which is corresponding to the theoretical analysis given before. The temperature changes the refractive index of the material and thus leads to the center wavelength shift. Based on the calculated effective mode refractive indices of the TE_0 and TE_1 modes across temperatures ranging from 7 to 295 K in Sect. 2, we fitted the data in Fig. 5(c) according to the formula:

$$\lambda_B(T) = (n_{eff0}(T) + n_{eff1}(T)) \times \Lambda. \quad (4)$$

Here, $\lambda_B(T)$, $n_{eff0}(T)$, and $n_{eff1}(T)$ are temperature-dependent parameters, and the grating period of the MWG Λ is the fitting parameter. The fitting lines are also given in Fig. 5(c),

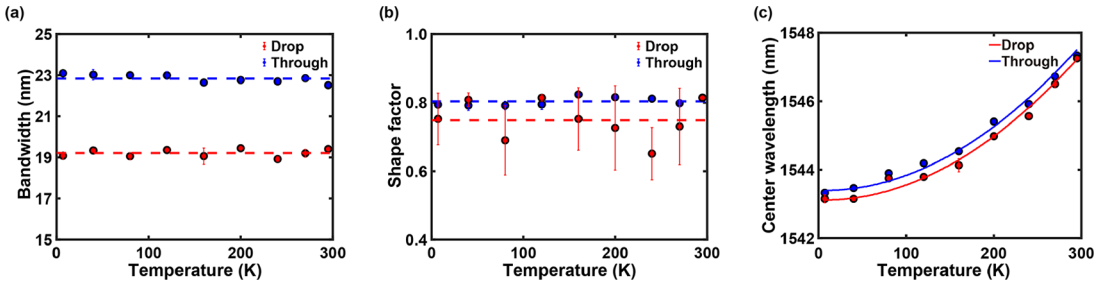

Fig. 5. Relationship between different parameters of the optical filter and the temperature. (a) Bandwidth variation of the spectra at drop and through ports according to the temperature, following the dotted lines as a guide to the eye. (b) Shape factor variation of the spectra at drop and through ports according to the temperature and the following guide lines. (c) Center wavelength variation of the spectra at drop and through ports according to the temperature and the fitting curves. Points are average results of multiple test, and error bars are mean squared errors.

and they are consistent well with the experimental results. The fitted grating period of the MWG according to the results at the drop port is $\Lambda_{drop} = 436.35 \pm 0.04$ nm, and the fitted value according to the results at the through drop is $\Lambda_{through} = 436.43 \pm 0.03$ nm, where the errors are the fitting standard errors. These fitted results are aligned with the designed grating period $\Lambda = 436.00$ nm.

Our work demonstrates that even under cryogenic conditions, the LNOI MWG filter still maintains its performance, which indicates the superior potential of the LNOI devices to operate effectively at cryogenic temperatures. The center wavelength shift is well explained by the material's refractive index variation with temperature, and this method will likely be further used to guide the design of various cryogenic devices. The large-scale integration of cryogenic compatible circuit including photonic sources, filters, modulators, and detectors will provide a compact solution for quantum optical systems and greatly reduce inter-chip connection losses, thus offering significant advantages in scalable photonic quantum information applications. The excellent material properties of the LNOI waveguide also offer a variety of possibilities for different applications such as on-chip manipulation atoms and connecting multiple cryogenic processors.

In conclusion, we prepare and characterize a LNOI MWG filter under cryogenic conditions. Experimental results show that the optical filter still has basically the same performance as that at room temperature, and just the center wavelength decreases by about 4 nm at 7 K compared to the results at 295 K. Furthermore, the center wavelength shift with temperature is explained through introducing the temperature-dependent effective index of the grating structure in the filter. These results will help to design different cryogenic compatible optical devices on the LNOI and further promote the full integration of quantum optical systems at cryogenic temperatures.

Funding. National Key Research and Development Program of China (2022YFA1204704); National Natural Science Foundation of China (12004373, 62061160487, 62275240, 62321166651, T2325022, U23A2074); Chinese Academy of Sciences Project for Young Scientists in Basic Research (YSBR-049); Research and Development Program of Anhui Province (2022b1302007); Fundamental Research Funds for the Central Universities.

Acknowledgment. This work was partially carried out at the USTC Center for Micro- and Nanoscale Research and Fabrication.

Disclosures. The authors declare no conflicts of interest.

Data availability. Data underlying the results presented in this paper are not publicly available at this time but may be obtained from the authors upon reasonable request.

REFERENCES

1. J. Wang, F. Sciarrino, A. Laing, *et al.*, Nat. Photonics **14**, 273 (2020).
2. L. Feng, M. Zhang, J. Wang, *et al.*, Photonics Res. **10**, A135 (2022).
3. S.-Y. Ren, W.-Q. Wang, Y.-J. Cheng, *et al.*, PhotoniX **4**, 12 (2023).
4. H.-S. Zhong, H. Wang, Y.-H. Deng, *et al.*, Science **370**, 1460 (2020).
5. S. Wang, Z.-Q. Yin, D.-Y. He, *et al.*, Nat. Photonics **16**, 154 (2022).
6. M. Zhang, L.-T. Feng, Z.-Y. Zhou, *et al.*, Light: Sci. Appl. **8**, 41 (2019).
7. L.-T. Feng, M. Zhang, D. Liu, *et al.*, Optica **10**, 105 (2023).
8. M. E. Grein, A. J. Kerman, E. A. Dauler, *et al.*, in *Advanced Photon Counting Techniques IX*, Vol. 9492 (SPIE, 2015), pp. 11–16.
9. X. Zhang, H.-O. Li, G. Cao, *et al.*, Nat. Sci. Rev. **6**, 32 (2019).
10. A. Niskanen, K. Harrabi, F. Yoshihara, *et al.*, Science **316**, 723 (2007).
11. B. Van Zeghbroeck, IEEE Trans. Appl. Supercond. **3**, 2881 (1993).
12. Y. Wei, S. Liu, X. Li, *et al.*, Nat. Nanotechnol. **17**, 470 (2022).
13. K. K. Mehta, C. D. Bruzewicz, R. McConnell, *et al.*, Nat. Nanotechnol. **11**, 1066 (2016).
14. N. A. Lange, J. P. Höpker, R. Ricken, *et al.*, Optica **9**, 108 (2022).
15. L. Feng, Y. Cheng, X. Qi, *et al.*, Optica **10**, 702 (2023).
16. M. Bartnick, M. Santandrea, J. P. Höpker, *et al.*, Phys. Rev. Appl. **15**, 024028 (2021).
17. F. Eltes, G. E. Villarreal-Garcia, D. Caimi, *et al.*, Nat. Mater. **19**, 1164 (2020).
18. U. Chakraborty, J. Carolan, G. Clark, *et al.*, Optica **7**, 1385 (2020).
19. M. Dong, G. Clark, A. J. Leenheer, *et al.*, Nat. Photonics **16**, 59 (2022).
20. F. Thiele, F. V. Bruch, V. Quiring, *et al.*, Opt. Express **28**, 28961 (2020).
21. E. Lomonte, M. A. Wolff, F. Beutel, *et al.*, Nat. Commun. **12**, 6847 (2021).
22. D. Liu, C. Zhang, D. Liang, *et al.*, Opt. Express **27**, 416 (2019).
23. C. Wang, Z. Li, M.-H. Kim, *et al.*, Nat. Commun. **8**, 2098 (2017).
24. B.-Y. Xu, L.-K. Chen, J.-T. Lin, *et al.*, Sci. China Phys. Mech. Astron. **65**, 294262 (2022).
25. V. Snigirev, A. Riedhauser, G. Lihachev, *et al.*, Nature **615**, 411 (2023).
26. S. Yuan, C. Hu, A. Pan, *et al.*, J. Semicond. **42**, 041304 (2021).
27. U. Schlarb and K. Betzler, Phys. Rev. B **48**, 15613 (1993).
28. J. He, D. Liu, B. Pan, *et al.*, Opt. Express **30**, 34140 (2022).
29. D. Dai and J. E. Bowers, Nanophotonics **3**, 283 (2014).
30. D. Dai, C. Li, S. Wang, *et al.*, Laser Photonics Rev. **12**, 1700109 (2018).
31. J. S. Browder and S. S. Ballard, Appl. Opt. **16**, 3214 (1977).
32. D. H. Jundt, Opt. Lett. **22**, 1553 (1997).
33. Y. Yanagase, S. Suzuki, Y. Kokubun, *et al.*, J. Lightwave Technol. **20**, 1525 (2002).